

# Laser-Driven Petahertz Electron Ratchet Nanobubbles

Luke Bhan, Cody L. Covington, and Kálmán Varga\*



Cite This: *Nano Lett.* 2022, 22, 4240–4245



Read Online

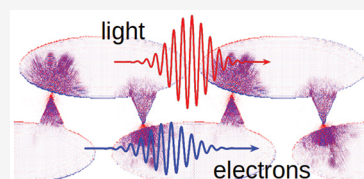
ACCESS |

Metrics & More

Article Recommendations

**ABSTRACT:** A laser-driven quantum electron ratchet nanodevice is proposed. The ratchet consists of a series of disconnected bubble-shaped nanodiode structures with a sharp tip to induce a large field enhancement. A laser pulse is used to create a plasmon oscillation in the vertical direction, and the shape of the bubble funnels the electrons toward the sharp tip leading to net electron transport in the horizontal direction. The electron current carries the fingerprint of the driving laser field. The system is modeled by using the time-dependent orbital free density functional theory with nanostructures containing thousands of atoms.

**KEYWORDS:** Ratchet, Nonequilibrium, Charge transport, Petahertz, Density functional theory, Femtosecond laser excitation



Electron ratchets produce directional currents from non-directional driving forces without an applied net bias. In practice, this is achieved by using time-dependent potentials to break time-reversal and spatial symmetries in the direction of transport.<sup>1–13</sup> Electron ratchets have been used for sensing (e.g., terahertz radiation see refs 9 and 14), for energy harvesting,<sup>15</sup> for solar cells,<sup>8</sup> or for converting AC currents or electronic noise to stable DC currents.<sup>16</sup> In addition to electrons, nanoscale ratchets can also transport atoms.<sup>3</sup>

The most frequently used mechanisms in ratchets are “flashing” and “tilting”. In flashing ratchets,<sup>1,10,13,17</sup> an asymmetric potential periodically moves the electrons between two states; in tilting ratchets, the source-drain bias oscillates with a time average of zero.<sup>18,19</sup> In these devices, various physical mechanisms lead to the ratchet effect including thermal excitation over energy barriers, tunneling through barriers, and wave reflection from barriers.

In this work, we propose and study a different electron ratchet based on laser-driven electron tunneling between sharp tips and flat surfaces. In this device, the direction of the electron transport and the driving laser is perpendicular. The generated time-dependent electron current oscillates at petahertz frequencies and is modulated by the frequency of the driving laser. The operation of the device is based on the observation<sup>20</sup> that an oscillating laser pulse tends to drive a net electron flux from a sharp tip to a flat surface. We have envisioned a periodic system of “nanobubbles” facing each other with a sharp tip as it is shown in Figure 1. Once the electrons are transported to the flat surface, they will be funneled to a sharp tip through a special bubble shape as a guide (see Figure 1). The same laser pulse then drives the electrons from the tip to the next bubble. The nanobubbles are not connected to each other, so the net electron current along the bubbles (*x*-direction in Figure 1) is solely due to the laser pulse acting in the perpendicular *z*-direction.

We have used the orbital-free time-dependent density functional theory (OF-TDDFT)<sup>21</sup> in our calculations. The

orbital-free density functional theory<sup>22–31</sup> is a suitable approach for large systems because its main variable is the electron density, and it computationally scales linearly with system size; it has been used in million-atom material simulations.<sup>32</sup> In a previous work, we have shown that the currents and induced fields predicted by OF-TDDFT calculations are in very good agreement with TDDFT calculations for jellium sheets, jellium spheres, atomistic sheets, and icosahedron clusters.<sup>21</sup>

The OF-TDDFT equation is a time-dependent Schrödinger equation for a single orbital<sup>21</sup>

$$\left(i\hbar\frac{\partial}{\partial t} - H_{OF}\right)\Psi(\mathbf{r}, t) = 0 \quad (1)$$

where

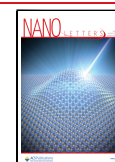
$$H_{OF}(\mathbf{r}, t) = -\frac{1}{2m}[-i\hbar\nabla_r + \mathbf{A}(\mathbf{r}, t)]^2 + V_{OF}[\rho](\mathbf{r}, t) \quad (2)$$

The density-dependent potential  $V_{OF}$  is a sum of the Hartree, the exchange correlation (local density approximation), the kinetic energy (Thomas–Fermi), and the atomic potentials. The von Weizsacker kinetic energy term is included in the kinetic energy of the time-dependent Schrödinger equation (eq 1). The atomic potentials are local pseudopotentials for the valence electrons. The carbon pseudopotential is generated for graphene using the approach of ref 33. The Al pseudopotential is taken from ref 34. The electron density and the electron current at time  $t$  are defined as

**Received:** April 6, 2022

**Revised:** May 9, 2022

**Published:** May 13, 2022



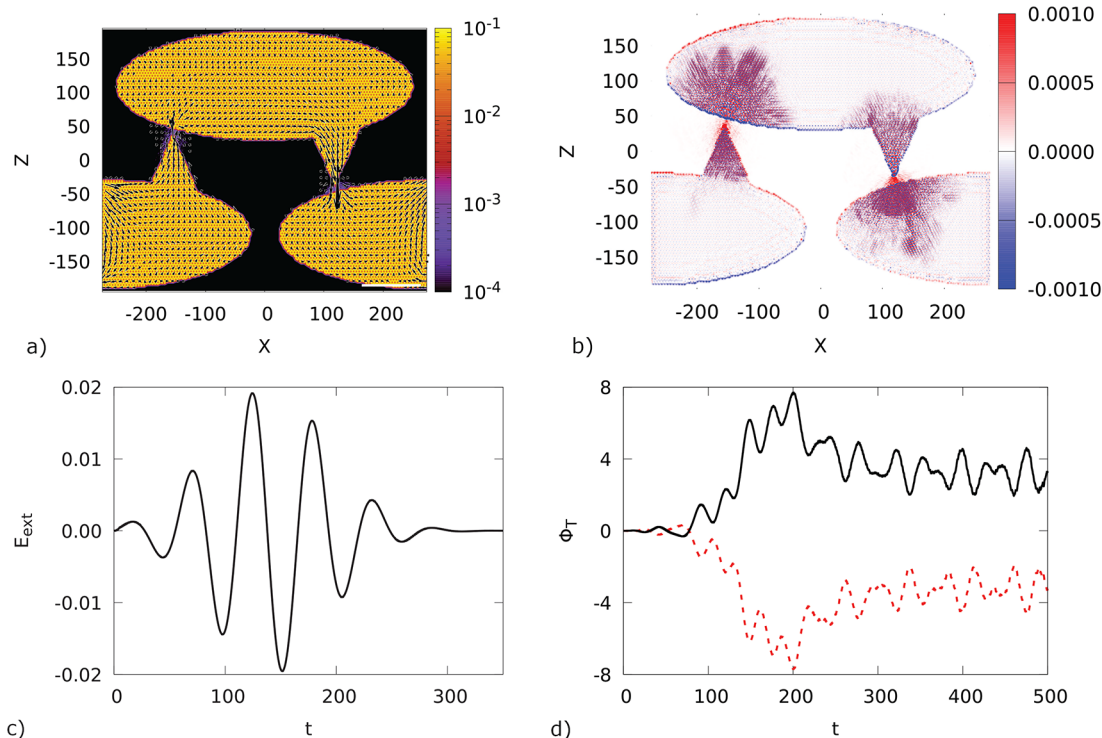


**Figure 1.** (a) Snapshots of the density with flux vectors. (b) Excited-state density difference. (c) Laser pulse and (d) total electron flux as a function of time for the large graphene nanobubble system (the red curve shows the flux when the system is inverted around the  $x$  axis). The vectors represent the summed electron flux with the white scale bar in the bottom right being 10 electrons. The ratchet has 14 064 atoms (56 256 electrons) in a box of  $N_x = 1148$ ,  $N_y = 16$ , and  $N_z = 810$  grid points with 0.478 au (0.253 Å) grid spacing. The time is in au, and 1. au corresponds to 0.024 fs. The gap size is about 1.4 nm.

$$\rho_{\text{OF}}(\mathbf{r}, t) = |\Psi(\mathbf{r}, t)|^2 \quad (3)$$

and

$$\mathbf{J}_{\text{OF}}(\mathbf{r}, t) = 2\text{Re}[\Psi(\mathbf{r}, t)^*(-i\hbar\nabla_{\mathbf{r}} + \mathbf{A}(\mathbf{r}, t))\Psi(\mathbf{r}, t)] \quad (4)$$

The wave function is represented on a real-space grid and is time-propagated using Taylor time evolution. A more detailed description can be found in ref 21. In the numerical calculation, first, the ground-state wave function is calculated by minimizing the energy of  $H_{\text{OF}}$  on a real-space grid. The parameters of the calculation are listed in the figure captions. The ground-state wave function is the starting wave function for the time propagation at  $t = 0$ .

A few-cycle, 7 fs long 400 nm laser pulse was used in the calculations with  $1.4 \times 10^{13}$  W/cm<sup>2</sup> (see Figure 1c). The strength of the laser field is chosen to keep the ionization minimal but induce a tunneling current in the gap region. This laser pulse is described by

$$E_z(\mathbf{r}, t) = E_0 \sin(\omega(t - x/c) + \phi) e^{-(t-t_0-x/c)^2/\alpha^2} \Gamma(t) \quad (5)$$

where  $\Gamma(t)$  is a ramping function that ensures that the electric field is zero at  $t = 0$ ,  $\alpha$  is the carrier-envelope width,  $\omega$  is the field frequency,  $E_0$  is the field strength, and  $\phi$  is the carrier-envelope phase. A  $\Delta t = 0.02$  au time step is used in the time propagation of the electron orbital.

To analyze the flow of electrons from one bubble to another, the flux of electrons through a given surface,  $S$  (for example, the  $y$ - $z$  plane), is calculated as

$$\Phi(t) = - \int_S d\mathbf{A} \cdot \mathbf{J}_{\text{OF}}(\mathbf{r}, t) \quad (6)$$

where the negative sign is used to give the electron flux. The flux can be integrated in time to give the net electron flow (summed flux) through the surface as

$$\Phi_T(t) = \int_0^T dt \Phi(t) \quad (7)$$

To study the electron flow, we defined a two-dimensional local flux vector by components

$$\Phi_x(x, z, t) = - \int_{yz} d\mathbf{A} \cdot \mathbf{J}_{\text{OF}}(\mathbf{r}, t) \quad (8)$$

$$\Phi_z(x, z, t) = - \int_{xy} d\mathbf{A} \cdot \mathbf{J}_{\text{OF}}(\mathbf{r}, t) \quad (9)$$

The flux vector is calculated in cells centered at point  $(x, z)$  using 20 grid points for the surface integrals in the  $y$ - $z$  or  $x$ - $y$  plane in the  $z$ - or  $x$ -direction and averaging over the  $y$ -direction. This flux vector can be plotted with the density snapshots to show the result of the ratchet action (see, e.g., Figure 1a). The flux vectors show the net amount of electron density that has passed through a region and its direction.

We will use two different systems as test examples; both are periodic in the  $x$ -direction which is the direction of the net electron transport. The first one is created from a graphene sheet (see Figures 1 and 2), and the second is a “clawlike” structure made of aluminum atoms (see Figure 3). Simulations were also performed on another aluminum ratchet made from repeating units of the same structure. This smaller ratchet uses a tip that is

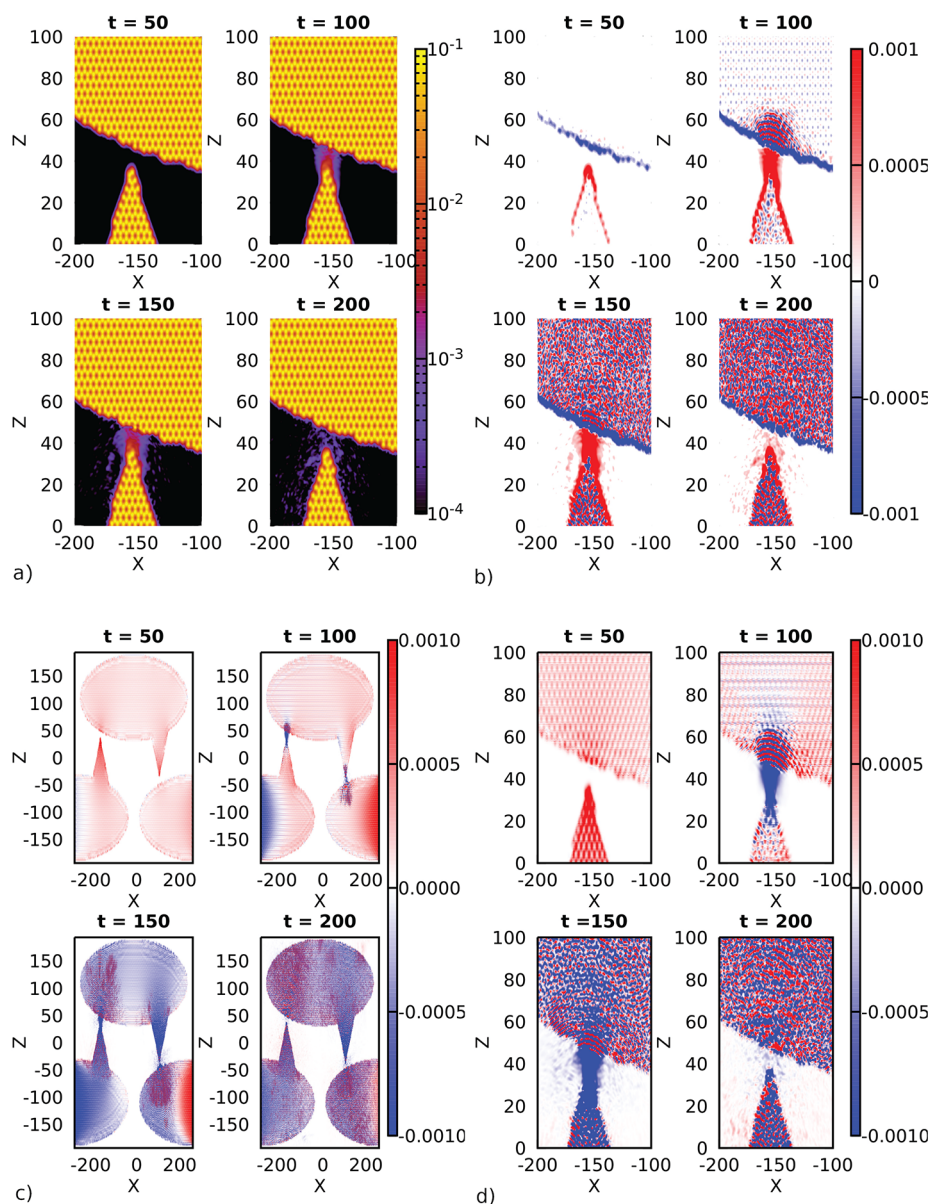


**Figure 2.** Graphene nanobubbles. (a) Snapshots of the electron density averaged in the  $y$ -direction. (b) Snapshots of the electrons density difference averaged over  $y$  zoomed in around the left tip. (c) Snapshots of the electron current averaged over  $y$ . (d) Snapshots of the electron current averaged over  $y$  zoomed in around the left tip. For other parameters, see the caption of Figure 1.

nearly perpendicular to the polarization of the exciting laser instead of two tips pointed in the direction of the laser.

Figure 1a shows a snapshot of the electron density and the current vectors elucidating the electron dynamics in the bubbles. The figure shows that the electrons flow from the tip of the lower bubble to the upper bubble, and in the upper bubble, it is channeled into the tip and transferred to the lower bubble. The same is illustrated in Figure 1b using the excited-state electron density. This density is obtained by subtracting the ground-state electron density from the time-dependent electron density. The excited-state density shows how the electrons flow from the tip to the bubble with interference like wave propagation superposed on the scattering patterns from the individual atoms. Figure 1d shows the total electron flux in the middle of the system. The flux increases with the laser and keeps oscillating even after the laser pulse is finished. These oscillations will diminish after the electrons become de-excited. The frequency

of the oscillations follows the oscillations of the laser pulse and in the petahertz range.

Figure 2 zooms in the snapshots of the time-dependent density and current in the graphene structure. The snapshots are taken when the laser amplitude has its maximum (not all snapshots are shown). Figure 2a shows the gap region and the tunneling of electrons. Figure 2b shows the excited-state electron density. One can see that the electrons mostly come from the top of the tip, but electrons also leave from the lower part of the tip. One can also notice that electrons are ejected from individual atoms. Figure 2c shows snapshots of the  $Z$  component of electron current. It is interesting that the current extends to the whole nanobubble. The tunneling current from the tip of the first bubble flows to the opposite side of the second bubble and is reflected back toward the tip of the second bubble. Zooming in to the gap region in Figure 2d, one can see that the tunneling current from the gap scatters on the atoms on the opposite surface showing wave interference-like features.

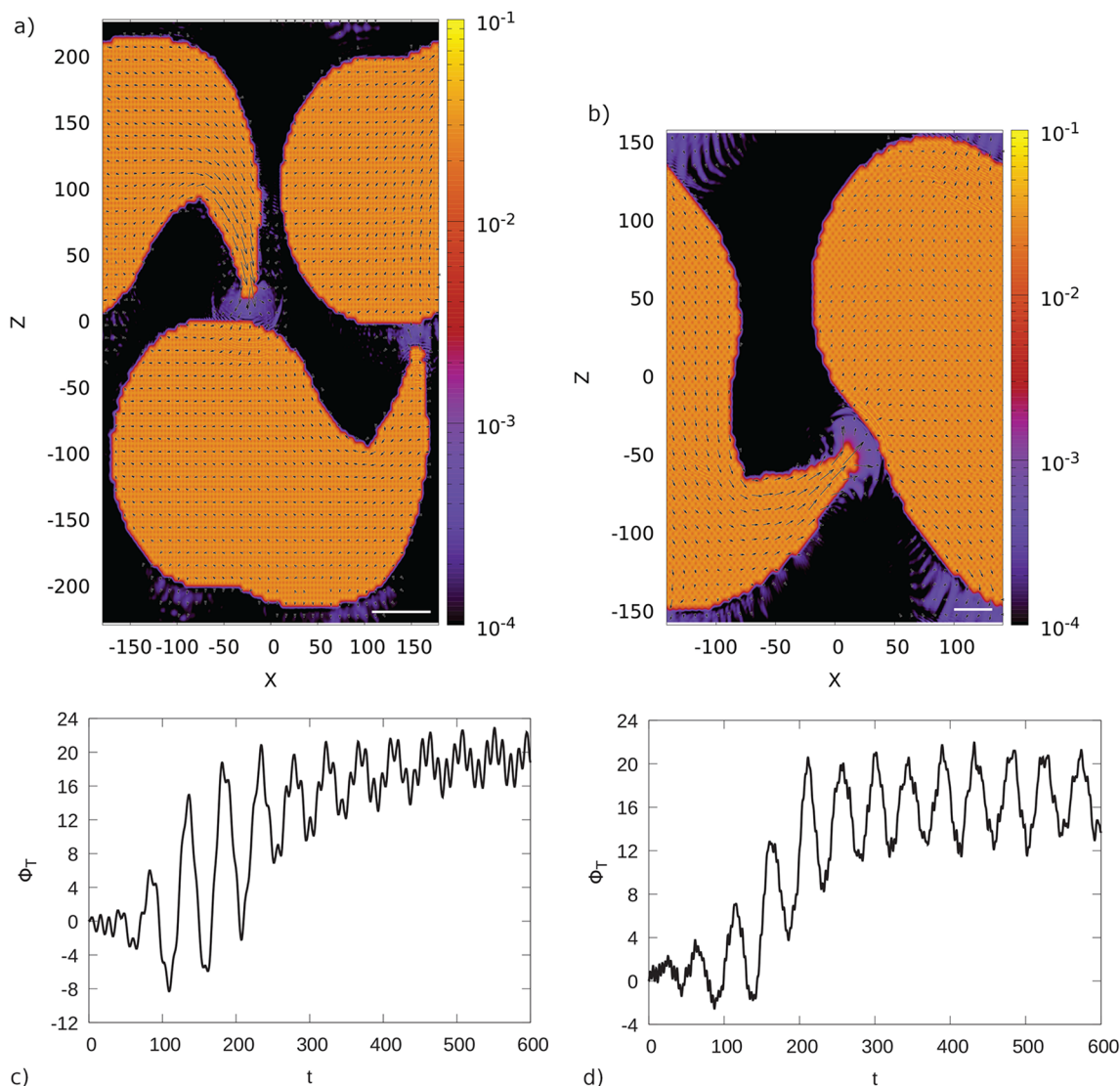


**Figure 3.** (a, b) Snapshots of the electron density for two different Al structures. (c, d) Total summed electron flux results throughout the simulation for the corresponding structures. Periodic boundary conditions are applied in all directions creating an infinite array of nanobubbles. The snapshots show an electron packet leaving the sharp tip and passing to the other side. The ratchet in panel a contains 7230 Al atoms (21 690 electrons), in a box with grid points  $N_x = 752$ ,  $N_y = 16$ , and  $N_z = 950$ , with a grid spacing of  $dx = 0.478$ . The smaller ratchet in panel b contains 3615 aluminum atoms (10 845 electrons), in a box with  $N_x = 592$ ,  $N_y = 16$ , and  $N_z = 655$  grid points, with a grid spacing of  $dx = 0.478$ . The gap size is about 1.2 nm.

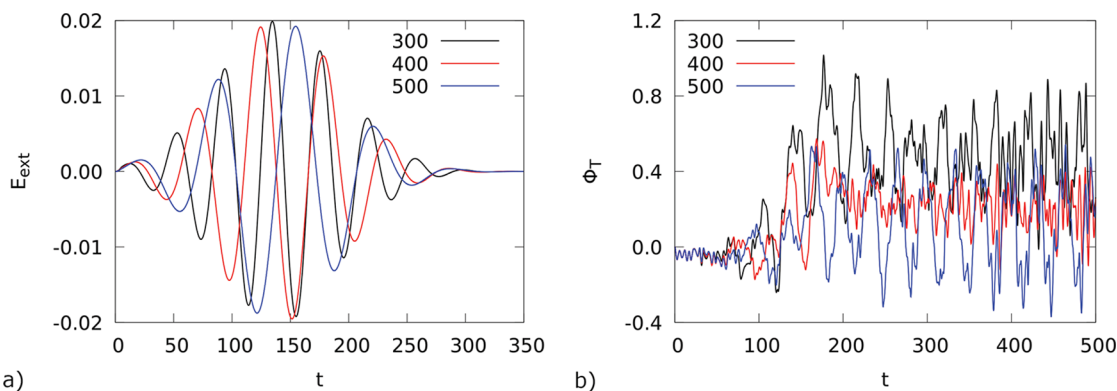


**Figure 4.** Wavelength dependence of the electron flux. (a) Laser pulses. (b) Summed flux. These calculations used the same shape as is shown in Figure 1, but the size is reduced to 3534 atoms (14 136 electrons) in a box with  $N_x = 584$ ,  $N_y = 16$ , and  $N_z = 440$  grid points with 0.478 au grid spacing.

Figure 3 shows the current flow in two different Al nanobubbles. Figure 3a,b clearly shows the electrons moving

from one bubble to the other one. The laser acts in the vertical  $z$ -direction, and the tips in these cases are pointing in a different

direction than the laser. However, that does not matter, as once the laser excites an oscillation in the structure, the electron current couples to the other direction due to the shape and angle of the lobe part. The tip has the greatest field enhancement, so that is where the electrons come off.

Figures 1d and 3c,d show the flux through the  $y$ - $z$  plane as a function of time in the nanobubble systems. The figures clearly show the net electron transport in the  $x$ -direction between the bubbles. The graphene system has a net rightward flow of about 3 electrons after the laser has ended. The aluminum structures have greater numbers of electrons transported, but the Al systems are also periodic in the  $y$ -direction. Figure 1d shows the summed flux for the  $x$ -mirrored system showing that the ratchet does behave as expected upon inversion of the structure. Also altering the phase of the laser pulse has very little effect on the ratchet properties of these systems, and a phase difference of  $180^\circ$  only produces slight differences in the summed flux curves.

Most interestingly, the tilted Al ratchet system produces the most net flow of electrons (Figure 3d). A potential cause for this is that the other structures rely on the laser field to transfer electrons between the structures. As the laser field is oscillatory, the electrons move back and forth to some extent. However, in the tilted Al ratchet, the laser field only excites the oscillation in the ratchet and does not drive the transport between the gap.

Finally, Figure 4 shows the dependence of the summed electron flux on the laser frequency. The electron flux decreases with the increasing wavelength. The flux is lower since fewer electrons are crossing in the gap when the frequency of the laser is higher. One can also see that the electron current is modulated by the laser frequency; the electron current oscillates at the petahertz scale. The magnitude of the flux depends on the shape of the bubble, and by testing different shapes, one can optimize the design for maximum flux.

The laser-induced electron current will disappear on a longer time scale for two main reasons. First, the electron current excites the electromagnetic fields, and the induced fields will reduce the currents. In an earlier work,<sup>20</sup> we have studied this effect, and we estimate that the reduction of current would be a factor of 2 for the present structures. Second, coupling to phonons would also have a damping effect, but the time scale of this de-excitation is much longer than the time of the ratchet effect in the present work.

In summary, we have shown that one can use laser pulses to drive electron current perpendicular to the direction of the laser in nanodiode-like quantum ratchets. On-chip petahertz electronic networks<sup>35–37</sup> using bowtie and other nanoantenna structures have been fabricated and experimentally measured, so the nanobubble system studied in this work seems to be a realistic approach. The nanobubble ratchet can be used for the detection of a carrier-envelope phase of optical pulses and developing optical frequency, petahertz electronics for high-speed information processing.

## AUTHOR INFORMATION

### Corresponding Author

Kálmán Varga – Department of Physics and Astronomy,  
Vanderbilt University, Nashville, Tennessee 37235, United States; [orcid.org/0000-0002-8093-1096](https://orcid.org/0000-0002-8093-1096);  
Email: [kalman.varga@vanderbilt.edu](mailto:kalman.varga@vanderbilt.edu)

### Authors

Luke Bhan – Department of Physics and Astronomy, Vanderbilt University, Nashville, Tennessee 37235, United States

Cody L. Covington – Department of Chemistry, Austin Peay State University, Clarksville, Tennessee 37044, United States

Complete contact information is available at:  
<https://pubs.acs.org/10.1021/acs.nanolett.2c01399>

## Notes

The authors declare no competing financial interest.

## REFERENCES

- (1) Kedem, O.; Lau, B.; Weiss, E. A. How To Drive a Flashing Electron Ratchet To Maximize Current. *Nano Lett.* **2017**, *17*, 5848–5854.
- (2) Ang, Y. S.; Ma, Z.; Zhang, C. Quantum ratchet in two-dimensional semiconductors with Rashba spin-orbit interaction. *Sci. Rep.* **2015**, *5*, 7872.
- (3) Salger, T.; Kling, S.; Hecking, T.; Geckeler, C.; Morales-Molina, L.; Weitz, M. Directed Transport of Atoms in a Hamiltonian Quantum Ratchet. *Science* **2009**, *326*, 1241–1243.
- (4) Linke, H.; Humphrey, T. E.; Löfgren, A.; Sushkov, A. O.; Newbury, R.; Taylor, R. P.; Omling, P. Experimental Tunneling Ratchets. *Science* **1999**, *286*, 2314–2317.
- (5) Ganichev, S. D.; Weiss, D.; Eroms, J. Terahertz Electric Field Driven Electric Currents and Ratchet Effects in Graphene. *Annalen der Physik* **2017**, *529*, 1600406.
- (6) Würger, A. Thermoelectric Ratchet Effect for Charge Carriers with Hopping Dynamics. *Phys. Rev. Lett.* **2021**, *126*, 068001.
- (7) Onishi, Y.; Isobe, H.; Nagaosa, N. Theory of Seebeck ratchet in a noncentrosymmetric electron-phonon coupled system. *Phys. Rev. B* **2021**, *104*, 155419.
- (8) Vaquero-Stainer, A.; Yoshida, M.; Hylton, N. P.; Pusch, A.; Curtin, O.; Frogley, M.; Wilson, T.; Clarke, E.; Kennedy, K.; Ekins-Daukes, N. J.; Hess, O.; Phillips, C. C. Semiconductor nanostructure quantum ratchet for high efficiency solar cells. *Communications Physics* **2018**, *1*, 7.
- (9) Olbrich, P.; et al. Terahertz ratchet effects in graphene with a lateral superlattice. *Phys. Rev. B* **2016**, *93*, 075422.
- (10) Lau, B.; Kedem, O.; Ratner, M. A.; Weiss, E. A. Identification of two mechanisms for current production in a biharmonic flashing electron ratchet. *Phys. Rev. E* **2016**, *93*, 062128.
- (11) Lau, B.; Kedem, O. Electron ratchets: State of the field and future challenges. *J. Chem. Phys.* **2020**, *152*, 200901.
- (12) Lehmann, J.; Kohler, S.; Hänggi, P.; Nitzan, A. Molecular Wires Acting as Coherent Quantum Ratchets. *Phys. Rev. Lett.* **2002**, *88*, 228305.
- (13) Kedem, O.; Lau, B.; Ratner, M. A.; Weiss, E. A. Light-responsive organic flashing electron ratchet. *Proc. Natl. Acad. Sci. U. S. A.* **2017**, *114*, 8698–8703.
- (14) Lau, B.; Kedem, O.; Kodaimati, M.; Ratner, M. A.; Weiss, E. A. A Silicon Ratchet to Produce Power from Below-Bandgap Photons. *Adv. Energy Mater.* **2017**, *7*, 1701000.
- (15) Hao, J.; Lu, H.; Nanayakkara, S. U.; Harvey, S. P.; Blackburn, J. L.; Ferguson, A. J. Perovskite Electronic Ratchets for Energy Harvesting. *Advanced Electronic Materials* **2020**, *6*, 2000831.
- (16) Hao, J.; Nanayakkara, S. U.; Tervo, E. J.; Blackburn, J. L.; Ferguson, A. J. High-performance carbon nanotube electronic ratchets. *Energy Environ. Sci.* **2021**, *14*, 5457–5468.
- (17) Roeling, E. M.; Germs, W. C.; Smalbrugge, B.; Geluk, E. J.; de Vries, T.; Janssen, R. A. J.; Kemerink, M. Organic electronic ratchets doing work. *Nat. Mater.* **2011**, *10*, 51–55.
- (18) Custer, J. P.; Low, J. D.; Hill, D. J.; Teitworth, T. S.; Christesen, J. D.; McKinney, C. J.; McBride, J. R.; Brooke, M. A.; Warren, S. C.; Cahoon, J. F. Ratcheting quasi-ballistic electrons in silicon geometric diodes at room temperature. *Science* **2020**, *368*, 177–180.
- (19) Linke, H.; Humphrey, T. E.; Lindelof, P. E.; Löfgren, A.; Newbury, R.; Omling, P.; Sushkov, A. O.; Taylor, R. P.; Xu, H. Quantum ratchets and quantum heat pumps. *Appl. Phys. A: Mater. Sci. Process.* **2002**, *75*, 237–246.

- (20) Bhan, L.; Covington, C.; Varga, K. Signatures of atomic structure in subfemtosecond laser-driven electron dynamics in nanogaps. *Phys. Rev. B* **2022**, *105*, 085416.
- (21) Covington, C.; Malave, J.; Varga, K. Coupled Maxwell and time-dependent orbital-free density functional calculations. *Phys. Rev. B* **2021**, *103*, 075119.
- (22) Witt, W. C.; del Rio, B. G.; Dieterich, J. M.; Carter, E. A. Orbital-free density functional theory for materials research. *J. Mater. Res.* **2018**, *33*, 777–795.
- (23) Mi, W.; Pavanello, M. Orbital-free density functional theory correctly models quantum dots when asymptotics, nonlocality, and nonhomogeneity are accounted for. *Phys. Rev. B* **2019**, *100*, 041105.
- (24) Shao, X.; Mi, W.; Pavanello, M. Efficient DFT Solver for Nanoscale Simulations and Beyond. *J. Phys. Chem. Lett.* **2021**, *12*, 4134–4139.
- (25) Shao, X.; Xu, Q.; Wang, S.; Lv, J.; Wang, Y.; Ma, Y. Large-scale ab initio simulations for periodic system. *Comput. Phys. Commun.* **2018**, *233*, 78–83.
- (26) Shao, X.; Jiang, K.; Mi, W.; Genova, A.; Pavanello, M. DFTpy: An efficient and object-oriented platform for orbital-free DFT simulations. *WIREs Computational Molecular Science* **2021**, *11*, No. e1482.
- (27) Mi, W.; Genova, A.; Pavanello, M. Nonlocal kinetic energy functionals by functional integration. *J. Chem. Phys.* **2018**, *148*, 184107.
- (28) Huang, C.; Libisch, F.; Peng, Q.; Carter, E. A. Time-dependent potential-functional embedding theory. *J. Chem. Phys.* **2014**, *140*, 124113.
- (29) Chen, M.; Jiang, X.-W.; Zhuang, H.; Wang, L.-W.; Carter, E. A. Petascale Orbital-Free Density Functional Theory Enabled by Small-Box Algorithms. *J. Chem. Theory Comput.* **2016**, *12*, 2950–2963.
- (30) Wang, Y. A.; Govind, N.; Carter, E. A. Orbital-free kinetic-energy functionals for the nearly free electron gas. *Phys. Rev. B* **1998**, *58*, 13465–13471.
- (31) Xia, J.; Carter, E. A. Density-decomposed orbital-free density functional theory for covalently bonded molecules and materials. *Phys. Rev. B* **2012**, *86*, 235109.
- (32) Hung, L.; Carter, E. A. Accurate simulations of metals at the mesoscale: Explicit treatment of 1 million atoms with quantum mechanics. *Chem. Phys. Lett.* **2009**, *475*, 163–170.
- (33) Kidd, D.; Umar, A. S.; Varga, K. Constrained density functional theory calculation with iterative optimization. *Phys. Rev. B* **2018**, *98*, 075108.
- (34) Huang, C.; Carter, E. A. Transferable local pseudopotentials for magnesium, aluminum and silicon. *Phys. Chem. Chem. Phys.* **2008**, *10*, 7109–7120.
- (35) Buckley, D.; Yang, Y.; Yang-Keathley, Y.; Berggren, K. K.; Keathley, P. D. Nanoantenna design for enhanced carrier-envelope-phase sensitivity. *J. Opt. Soc. Am. B* **2021**, *38*, C11–C21.
- (36) Yang, Y.; Turchetti, M.; Vasireddy, P.; Putnam, W. P.; Karnbach, O.; Nardi, A.; Kärtner, F. X.; Berggren, K. K.; Keathley, P. D. Light phase detection with on-chip petahertz electronic networks. *Nat. Commun.* **2020**, *11*, 3407.
- (37) Bionta, M. R.; Ritzkowski, F.; Turchetti, M.; Yang, Y.; Cattozzo Mor, D.; Putnam, W. P.; Kärtner, F. X.; Berggren, K. K.; Keathley, P. D. On-chip sampling of optical fields with attosecond resolution. *Nat. Photonics* **2021**, *15*, 456–460.